IEEE Access
Multidisciplinary ⋮ Rapid Review ⋮ Open Access Journal

Received November 11, 2021, accepted November 22, 2021, date of publication November 25, 2021,
date of current version December 6, 2021.

Digital Object Identifier 10.1109/ACCESS.2021.3131127

Error Performance Analysis of Access Point-Based Reconfigurable Intelligent Surfaces in the Presence of Gaussian-Plus-Laplacian Additive Noise

NARUSHAN PILLAY, (Member, IEEE), AND HONGJUN XU, (Member, IEEE)
School of Engineering, University of KwaZulu-Natal, Durban 4041, South Africa
Corresponding author: Narushan Pillay (pillayn@ukzn.ac.za)

ABSTRACT In this paper, we investigate the error performance of access point-based reconfigurable intelligent surfaces (AP-RISs) under a Rayleigh frequency-flat slow fading channel with path loss in the presence of Gaussian-plus-Laplacian additive noise. Since the additive noise includes an impulsive Laplacian component, it describes a scenario that is more realistic in practice. A closed-form expression of the average bit error probability (ABEP) is derived and validated by simulation results. The ABEP formulation employs an approximation of the sum of Rayleigh random variables and agrees well with simulation results for arbitrary surface sizes. However, the ABEP expression takes relatively long to evaluate due to the required multiple computations of the confluent hypergeometric function. On this note, a simplified expression of the ABEP is formulated by employing an asymptotic cumulative distribution function representation of the Gaussian-plus-Laplacian noise. The simplified ABEP agrees well with simulation results. An asymptotic analysis of the ABEP shows that the asymptotic diversity order is not affected by the Laplacian component. Finally, the ABEP formulations are used in the validations of error performance for an AP-RIS-assisted two-way relaying network under the same channel conditions. Overall, the investigations in this paper demonstrates the vulnerability of RISs to this type of noise and highlights the need for the design of suitable mitigation techniques.

INDEX TERMS Access point-based reconfigurable intelligent surfaces, Gaussian-plus-Laplacian additive noise, impulsive noise, intelligent reflecting surfaces, heavy-tail distributions, two-way relaying.

I. INTRODUCTION

The use of smart propagation in next generation networks is currently showing much promise in the research community and future releases of fifth- and sixth-generation wireless communications technology may exploit these concepts. A very recent example of smart propagation is the phase-adjustable element reconfigurable intelligent surface (RIS) that has been proposed as a subset of RISs or intelligent reflecting surfaces [1]. An RIS is able to intelligently modify an impinging electromagnetic wave to enhance communications system objectives, including, but not limited to, reliability, capacity, energy and spectrum efficiency [1], [2]. The generic RIS is made up of a large number of low-cost and energy-efficient reflecting elements. Elements are associated with an adjustable parameter that may be software-defined, for example, amplitude, phase, frequency or polarization. Phase-adjustable RISs are very attractive because they can be passive and hence, low cost and can enable the superposition of several coherent reflected signals at the receiver [1]–[3]. This ensures that the average signal-to-noise ratio (SNR) increases proportionally to the square of the number of RIS elements, thus significantly increasing the SNR especially for large element RISs.

Some very recent contributions in the literature are: Since co-channel interference can severely degrade the received signal, its effect on a RIS-assisted dual-hop mixed free-space optical-radio frequency (RF) communication system has been considered [4]. It is further demonstrated that the system still gains significant performance enhancement compared to its traditional counterpart. In [5], a RIS-assisted Alamouti scheme which employs only a single RF signal generator at

The associate editor coordinating the review of this manuscript and approving it for publication was Razi Iqbal.

the transmitter is proposed. It is shown that the diversity order is preserved compared to the classical Alamouti scheme. Furthermore, a RIS-assisted and index modulation-based vertical Bell Labs layered space-time scheme is proposed and supported by optimal and sub-optimal detectors. In [6], a simple yet effective model for RIS scattering is proposed and used to formulate an expression for path loss of the transmitter-RIS-receiver channel. The potential of RISs in anti-jamming communications is investigated in [7], by considering an aerial RIS (ARIS) that is deployed in the air for jamming mitigation. Optimization frameworks for ARIS deployment and passive beamforming are proposed and results show that legitimate transmissions are effectively enhanced.

One of the key open challenges to the realization of RISs is the acquisition of channel state information [3], since the channel knowledge is a critical component in the transceiver design of RIS-assisted communications to achieve its full potential. Base station (BS)-User RIS-assisted communication requires channel knowledge pertaining to a cascaded channel, since estimation of the User-RIS and BS-RIS links are required [3]. On this note, several solutions involving active channel sensors, channel decomposition and structural learning are currently being investigated [3].

Meanwhile, an access point (AP)-based RIS (AP-RIS) was conceptualized [8] to allow both information transmission and phase adjustment, while retaining the use of passive and low-cost reflecting elements. An AP-RIS is realized by placing an RF source in very close proximity to an RIS. This inherently eliminates the cascaded channel and only knowledge of the User-RIS link is required; hence, naturally holding much promise in terms of reduced system complexity.

Conventionally, wireless communication systems are assumed to be affected by only Gaussian noise. However, in practical scenarios or particular environments, such as metropolitan, manufacturing plants and indoor settings, the noise can have an impulsive component [9]. This component of the noise can occur in transients or bursts and is sporadic/non-contiguous in nature, resulting in the serious degradation of reliability or error performance. Man-made and natural sources that are responsible for generating the impulsive component in wireless communication systems include, but are not limited to, ignition noise in motor vehicles, switching transients in power lines, fluorescent lighting, multiple-access interference and lightning discharges; hence, resulting in distributions with positive excess-Kurtosis (heavy-tails) [10]. These distributions are more accurately described by models, such as the Symmetric-alpha Stable (SαS) which includes the Cauchy ($\alpha = 1$) distribution, Middleton Class A and Class B, generalized Gaussian, Laplacian and Bernoulli-Gaussian [9]–[11].

In [11], an analysis of diversity-reception schemes in the presence of additive noise including an impulsive component is presented, where the additive noise assumes a Gaussian-plus-Laplacian model. The Laplacian distribution is assumed over other impulsive noise models, due to its convenient analytical properties.

A. MOTIVATION AND CONTRIBUTIONS

Impulsive noise can have a significant deleterious effect on the error performance of wireless communication systems [9]–[11]. In the current open literature, there has been no investigation into the effect of additive noise with an impulsive component on the error performance of RIS-assisted communications. On this note, since the AP-RIS[1] holds much promise due its low system complexity, we consider the vulnerability of its error performance to additive noise with an impulsive component.

Due to the convenient analytical properties of the Laplacian distribution which may be used to model the impulsive noise component, we consider a mixture of Gaussian and Laplacian additive noise and study it's effect on the error performance of AP-RIS-assisted communications.

Based on the above, the contributions of this paper[2] are as follows: a) We derive the theoretical average bit error probability (ABEP) of an AP-RIS for a Rayleigh frequency-flat slow fading channel with path loss in the presence of Gaussian-plus-Laplacian additive noise. The formulation employs an approximation of the sum of Rayleigh random variables (RVs) and therefore agrees well for arbitrary RIS sizes. b) An asymptotic analysis is presented and includes the formulation of a simplified ABEP expression using an asymptotic representation of the cumulative distribution function (CDF) of the additive noise, and c) The formulated ABEPs are further used in the validations of error performance of a two-way relaying network under the same channel conditions.

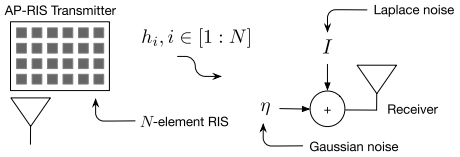

FIGURE 1. Model of the AP-RIS transmitter-receiver system.

II. SYSTEM MODEL AND PRELIMINARIES

Consider an AP-RIS transmitter and receiver as depicted in Fig. 1. The RIS at the transmitter is equipped with N elements and the transmitter and receiver each make use of a single RF antenna. The antenna at the transmitter is located sufficiently

[1] In [8], [12] analyses of the error performance of AP-RISs under a frequency-flat Rayleigh fading channel in the presence of Gaussian-only additive noise have been investigated. Unlike the analysis in [8], which makes the simplifying assumption of large RISs, the analysis in [12] is valid even for small RISs.

[2] *Notation*: $|\cdot|$ is the Euclidean norm, $E\{\cdot\}$ is the expectation operator, while $Q(\cdot)$ represents the Gaussian Q-function. $\binom{\cdot}{\cdot}$ is the binomial coefficient. $(\cdot)!$ represents factorial and $(2N-1)!! = (2N-1)(2N-3)\cdots 3\cdot 1$ represents the double factorial. $\mathcal{I}_p$ represents an integral p. $\oplus$ represents the XOR operation. j is the complex number $\sqrt{-1}$.

close to the RIS, such that there is no small-scale fading channel between the antenna and the RIS [8].

Assuming a Rayleigh frequency-flat slow fading channel with path loss in the presence of Gaussian-plus-Laplacian additive noise at the receiver, the received signal may be defined as:

$$r = \sqrt{\gamma P_L}\left[\sum_{i=1}^{N} h_i e^{j\phi_i}\right]\xi + I + \eta = \sqrt{\gamma P_L}\sum_{i=1}^{N}\alpha_i\xi + I + \eta, \tag{1}$$

where the RV h_i is distributed as $C\mathcal{N}(0, 1)$ with Rayleigh distributed magnitude α_i and uniformly distributed phase θ_i, such that $h_i = \alpha_i e^{j\theta_i}$ represents the channel between the receive antenna and the i-th, $i \in [1 : N]$ RIS element, ϕ_i represents the adjustable phase at the i-th RIS element and is set as $\phi_i = -\theta_i$, such as to maximize the received SNR [8], ξ is the message carrying binary phase shift keying (BPSK) symbol and $E\{\xi^2\} = 1$. The average transmit power is γ and P_L is the total path loss [5], [6], which is defined in Section IV. The Laplacian and Gaussian additive noise components are represented by I and η, respectively. Both I and η are mutually independent and have probability density functions (PDFs) given by (2.1) and (2.2), respectively.

$$f_I(x) = \frac{1}{2c}e^{-\frac{|x|}{c}}, \tag{2.1}$$

$$f_\eta(x) = \frac{1}{\sqrt{2\pi}\sigma}e^{-\frac{x^2}{2\sigma^2}}, \tag{2.2}$$

where c, $c > 0$ is a scale parameter of the Laplacian distribution and σ, $\sigma > 0$ is the scale parameter (standard deviation) of the Gaussian distribution.

In the upper part of Fig. 2 (refer to the top of the next page), we plot the empirical[3] versus analytical PDFs of I for $c = 0.8$, 1, 2 and 4. The analytical PDF of the Gaussian distribution given by (2.2) with $\sigma = 1$, is also depicted and serves to give an indication of the positive excess kurtosis of the Laplacian distributed noise. It is evident that the empirical and analytical PDFs of I agree well and as c increases from $c = 0.8$ to $c = 4$ the heaviness of the tails increase, i.e. the noise takes on extreme values with increasing frequency.

The PDF of the total additive noise given by $J = I + \eta$ was determined in [13], and is defined as:

$$f_J(x, \sigma, c) = \frac{1}{2c}e^{\frac{\sigma^2}{2c^2}}\left[e^{\frac{x}{c}}Q\left(\frac{x}{\sigma} + \frac{\sigma}{c}\right) + e^{-\frac{x}{c}}Q\left(-\frac{x}{\sigma} + \frac{\sigma}{c}\right)\right]. \tag{3}$$

In the lower part of Fig. 2, the empirical versus analytical PDF plots of J for $c = 0.8$, 1, 2 and 4 assuming $\sigma = 1$ are shown and agree well. Once again, the Gaussian PDF ($\sigma = 1$) is depicted. While the Gaussian-plus-Laplacian PDF peaks are less sharp, as expected the positive excess kurtosis remains evident. Since, there is a high probability of extreme Gaussian-plus-Laplacian noise amplitudes occurring, this suggests the potentially significant deleterious impact this noise will have on error performance. In the ensuing analysis, we will employ the PDF given by (3).

[3]The empirical PDFs were generated from simulated noise using the histogram function $hist(\cdot)$ in MATLAB. A Laplacian RV with scale parameter c was simulated using $I = -c \times sign(u)\ln(1 - 2|u|)$, where $u = -0.5 + rand(\cdot)$ is a uniformly distributed RV and $sign(\cdot)$, $rand(\cdot)$ are the signum, uniform RV functions, respectively, in MATLAB.

III. ERROR PERFORMANCE ANALYSIS

A. THEORETICAL ABEP

Consider an equivalent received signal model of (1) given as $r = x\xi + \bar{I} + \bar{\eta}$, where $x = \sum_{i=1}^{N}\alpha_i/\sqrt{N}$, $\bar{I}$ has scaling parameter $\bar{c} = \frac{c}{\sqrt{\gamma P_L N}}$ and $\bar{\eta}$ has scaling parameter $\bar{\sigma} = \frac{\sigma}{\sqrt{\gamma P_L N}}$.

Then with BPSK transmission, the ABEP of the AP-RIS system for a Rayleigh frequency-flat slow fading channel with path loss in the presence of Gaussian-plus-Laplacian additive noise may be given as:

$$P_e = \int_0^\infty P(\bar{I} + \bar{\eta} > x) f_x(x)\mathrm{d}x, \tag{4}$$

where $f_x(x)$ the PDF of x may be approximated[4] as [14]:

$$f_x(x) \approx \frac{x^{2N-1}e^{\frac{-x^2}{2b}}}{2^{N-1}b^N(N-1)!}, \tag{5}$$

with $b = \frac{1}{2N}[(2N-1)!!]^{\frac{1}{N}}$.

Using $P(\bar{I} + \bar{\eta} > x) \triangleq 1 - F_{\bar{J}}(x, \bar{\sigma}, \bar{c})$, where $F_{\bar{J}}(x, \bar{\sigma}, \bar{c})$ is the CDF of $\bar{J} = \bar{I} + \bar{\eta}$, which is defined as [11]:

$$F_{\bar{J}}(x, \bar{\sigma}, \bar{c}) = \frac{e^{\frac{\sigma^2}{2c^2}}}{2}\left[e^{\frac{x}{\bar{c}}}Q\left(\frac{x}{\bar{\sigma}} + \frac{\sigma}{c}\right) - e^{-\frac{x}{\bar{c}}}Q\left(-\frac{x}{\bar{\sigma}} + \frac{\sigma}{c}\right)\right] - Q\left(\frac{x}{\bar{\sigma}}\right) + 1, \tag{6}$$

we may rewrite (4) as:

$$P_e \approx \frac{1}{2^{N-1}b^N(N-1)!}\left\{\int_0^\infty x^{2N-1}e^{-\frac{x^2}{2b}}\mathrm{d}x - \mathcal{I}_1\right\}, \tag{7}$$

where $\mathcal{I}_1 = \int_0^\infty x^{2N-1}e^{-\frac{x^2}{2b}}F_{\bar{J}}(x, \bar{\sigma}, \bar{c})\mathrm{d}x$.

Using integration-by-parts, $\mathcal{I}_1$ is given as (given in Appendix A):

$$\mathcal{I}_1 = \frac{(N-1)!}{2^{1-N}b^{-N}}\left[\frac{1}{2} + \sum_{k=0}^{N-1}\frac{1}{k!(2b)^k}\mathcal{I}_2\right], \tag{8}$$

where $\mathcal{I}_2 = \int_0^\infty x^{2k}e^{-\frac{x^2}{2b}}f_{\bar{J}}(x, \bar{\sigma}, \bar{c})\mathrm{d}x$ and may be solved as (given in Appendix B):

$$\mathcal{I}_2 = \frac{1}{2\bar{c}}e^{-0.5\varphi_2^2(\varphi_1+1)}\bar{\sigma}^{2k+1}\sum_{m=0}^{2k}(-1)^{2k-m} \times \binom{2k}{m}\varphi_2^{2k-m}\mathcal{I}_3, \tag{9}$$

where $\mathcal{I}_3 = \int_{-\infty}^{\infty}e^{-0.5\varphi_1 y^2}e^{\varphi_2(\varphi_1+1)y}y^m Q(y)\mathrm{d}y$ with $\varphi_1 = \frac{\bar{\sigma}^2}{b}$, $\varphi_2 = \frac{\sigma}{c}$ and using the identity $Q(-y) = 1 - Q(y)$, may be

[4]A more accurate expression of the PDF $f_x(x)$ was given as Equ. (9) in [14] but makes negligible difference to the accuracy here. Comparison is drawn in Section IV.

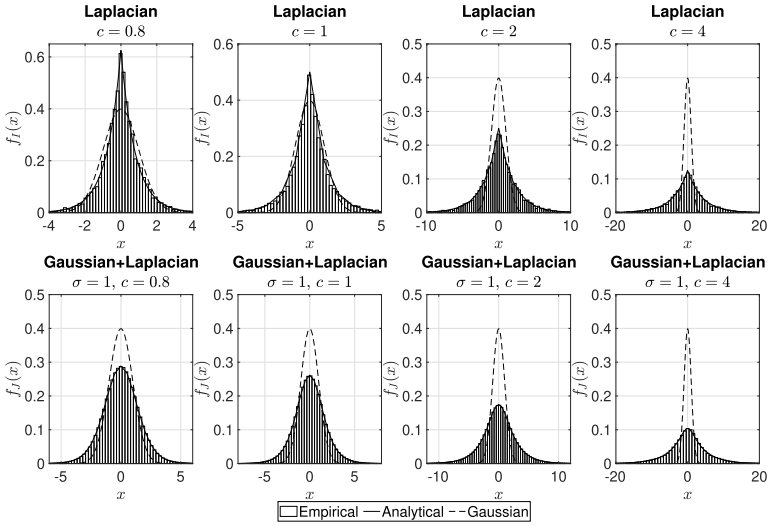

FIGURE 2. Empirical versus analytical PDFs for Laplacian ($c = 0.8, 1, 2, 4$) and Gaussian-plus-Laplacian ($\sigma = 1$, $c = 0.8, 1, 2, 4$) noises with Gaussian PDF ($\sigma = 1$) indicated.

equivalently[5] written as:

$$\mathcal{I}_3 = \mathcal{I}_{31} + \mathcal{I}_{32}, \tag{10}$$

where $\mathcal{I}_{31} = \int_0^\infty e^{-0.5\varphi_1 y^2} e^{\varphi_2(\varphi_1+1)y} y^m Q(y)\mathrm{d}y$ and $\mathcal{I}_{32} = \int_0^\infty e^{-0.5\varphi_1 y^2} e^{-\varphi_2(\varphi_1+1)y}(-y)^m[1-Q(y)]\mathrm{d}y$.

Applying the trapezoidal rule to $Q(\cdot)$, we get:

$$Q(y) \approx \frac{1}{2n}\left[\frac{1}{2}e^{-\frac{y^2}{2}} + \sum_{\ell=1}^{n-1}\exp\left(-\frac{y^2}{2\sin^2\left(\frac{\ell\pi}{2n}\right)}\right)\right], \tag{11}$$

where $n \geq 2$ is the number of intervals used in the integration; accordingly, we write $\mathcal{I}_{31}$ as:

$$\begin{aligned}\mathcal{I}_{31} &\approx \frac{1}{4n}\int_0^\infty e^{-y^2(0.5\varphi_1+0.5)} e^{y\varphi_2(\varphi_1+1)} y^m \mathrm{d}y \\ &\quad + \frac{1}{2n}\sum_{\ell=1}^{n-1}\int_0^\infty e^{-y^2\left(0.5\varphi_1+\frac{1}{2\sin^2\left(\frac{\ell\pi}{2n}\right)}\right)} e^{y\varphi_2(\varphi_1+1)} y^m \mathrm{d}y.\end{aligned} \tag{12}$$

Using [15, Equ. (3.462.1)], (12) is reduced to:

$$\begin{aligned}\mathcal{I}_{31} &\approx \frac{\Gamma(v)}{4n}(2\beta_1)^{-v/2}\exp\left(\frac{\rho^2}{8\beta_1}\right)D_{-v}\left(\frac{\rho}{\sqrt{2\beta_1}}\right) \\ &\quad + \frac{\Gamma(v)}{2n}\sum_{\ell=1}^{n-1}(2\beta_2^\ell)^{-v/2}\exp\left(\frac{\rho^2}{8\beta_2^\ell}\right)D_{-v}\left(\frac{\rho}{\sqrt{2\beta_2^\ell}}\right),\end{aligned} \tag{13}$$

where $\beta_1 = 0.5(\varphi_1+1)$, $\beta_2^\ell = 0.5\left(\varphi_1 + \frac{1}{\sin^2\left(\frac{\ell\pi}{2n}\right)}\right)$, $\rho = -\varphi_2(\varphi_1+1)$, $v = m+1$ and $D_{-v}(\cdot)$ is the parabolic cylinder function [15], which is defined as:

$$D_{-v}(z) = \frac{e^{-z^2/4}}{\Gamma(v)}\int_0^\infty e^{-xz-0.5x^2}x^{v-1}\mathrm{d}x, \tag{14}$$

and in terms of the confluent hypergeometric function ${}_1F_1(\cdot;\cdot;\cdot)$ as [15]:

$$\begin{aligned}D_{-v}(z) = 2^{-v/2}e^{-z^2/4}\Bigg\{&\frac{\sqrt{\pi}}{\Gamma\left(\frac{1+v}{2}\right)}\,{}_1F_1\left(\frac{v}{2};\frac{1}{2};\frac{z^2}{2}\right) \\ &-\frac{\sqrt{2\pi}z}{\Gamma\left(\frac{v}{2}\right)}\,{}_1F_1\left(\frac{1+v}{2};\frac{3}{2};\frac{z^2}{2}\right)\Bigg\}.\end{aligned} \tag{15}$$

Similar to the steps used to arrive at (13), we may determine the solution of $\mathcal{I}_{32}$ in (10) as:

$$\begin{aligned}\mathcal{I}_{32} \approx\ &(-1)^m\Gamma(v)(2\beta_3)^{-v/2}\exp\left(\frac{\rho^2}{8\beta_3}\right)D_{-v}\left(\frac{-\rho}{\sqrt{2\beta_3}}\right) \\ &-(-1)^m\frac{\Gamma(v)}{4n}(2\beta_1)^{-v/2}\exp\left(\frac{\rho^2}{8\beta_1}\right)D_{-v}\left(\frac{-\rho}{\sqrt{2\beta_1}}\right) \\ &-(-1)^m\frac{\Gamma(v)}{2n}\sum_{\ell=1}^{n-1}(2\beta_2^\ell)^{-v/2}\exp\left(\frac{\rho^2}{8\beta_2^\ell}\right)D_{-v}\left(\frac{-\rho}{\sqrt{2\beta_2^\ell}}\right),\end{aligned} \tag{16}$$

where $\beta_3 = 0.5\varphi_1$.

Solving the first term in (7) using [15, Equ. (3.326.2)] and substituting in turn (8), (9), (10), (13) and (16) in (7), then simplifying, we finally arrive at the approximate ABEP expression as:

$$\begin{aligned}P_e \approx\ &\frac{\Gamma(N)}{(N-1)!} - \frac{1}{8n}\varphi_2 e^{-0.5\varphi_2^2(\varphi_1+1)}\sum_{k=0}^{N-1}\frac{\bar{\sigma}^{2k}}{k!\,(2b)^k} \\ &\times\sum_{m=0}^{2k}(-1)^{2k-m}\binom{2k}{m}\varphi_2^{2k-m}2^{-\frac{v}{2}}\Gamma(v)\Bigg\{\beta_1^{-v/2}\exp\left(\frac{\rho^2}{8\beta_1}\right)\end{aligned}$$

[5]Note, we assumed the integration interval $(-\infty, \infty)$ for convenience in derivation of (9); however, we now convert back to the interval $(0, \infty)$, since we subsequently employ an approximation of $Q(\cdot)$ to solve $\mathcal{I}_3$.

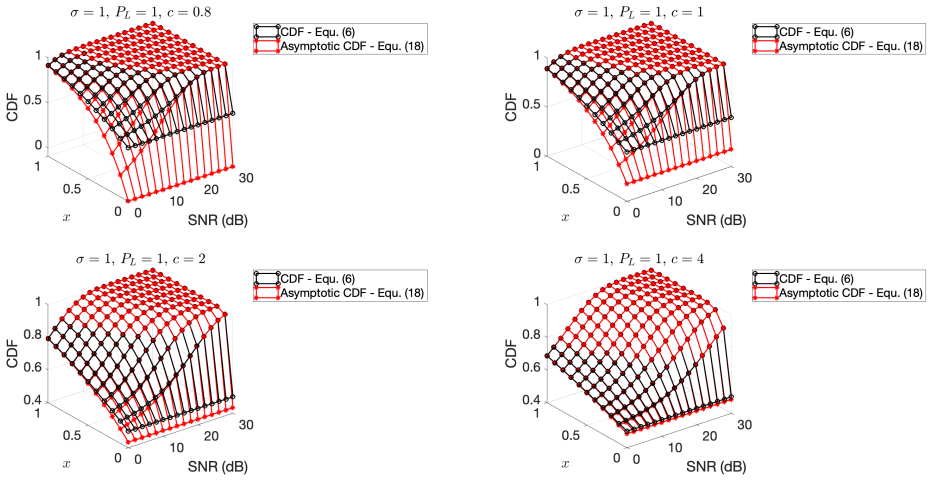

FIGURE 3. Comparison of CDFs ($\sigma = 1$, $c = 0.8, 1, 2, 4$) showing accuracy of asymptotic CDF (18) with $N = 4$, $P_L = 1$.

$$\times\left[D_{-v}\left(\frac{\rho}{\sqrt{2\beta_1}}\right)-(-1)^m D_{-v}\left(\frac{-\rho}{\sqrt{2\beta_1}}\right)\right]+2\sum_{\ell=1}^{n-1}(\beta_2^{\ell})^{-v/2}$$
$$\times\exp\left(\frac{\rho^2}{8\beta_2^{\ell}}\right)\left[D_{-v}\left(\frac{\rho}{\sqrt{2\beta_2^{\ell}}}\right)-(-1)^m D_{-v}\left(\frac{-\rho}{\sqrt{2\beta_2^{\ell}}}\right)\right]$$
$$+(-1)^m(4n)\beta_3^{-v/2}\exp\left(\frac{\rho^2}{8\beta_3}\right)D_{-v}\left(\frac{-\rho}{\sqrt{2\beta_3}}\right)\Bigg\}-\frac{1}{2}. \tag{17}$$

B. ASYMPTOTIC ANALYSIS

1) SIMPLIFIED ABEP USING AN ASYMPTOTIC CDF

The ABEP expression derived in (17) requires multiple computations of the confluent hypergeometric function, which is well-known to be relatively slow. By evaluating (7) using an asymptotic representation of (6), (17) may be simplified. Setting $\gamma \to \infty$, it may be validated that (6) may be approximated as:

$$F_{\bar{J}}^{\gamma\to\infty}(x,\bar{\sigma},\bar{c}) \approx 1-\frac{\exp\left(\frac{\sigma^2}{2c^2}\right)}{2}e^{\frac{-x}{\bar{c}}}. \tag{18}$$

Fig. 3 illustrates the curves of the CDF given by (6) and the asymptotic CDF given by (18). We have considered values of $c = 0.8, 1, 2$ and 4. Further, we have only considered $N = 4$, which represents the worst-case setting. It is immediately evident that at high SNRs, the CDFs match exactly. For example, in the case of $c = 0.8$, for small values of x the match is very tight from a worst case SNR of approximately 16 dB, while at higher values of x the match is tight even in the low SNR region. As c increases from $c = 1$ to $c = 4$, the match becomes tighter even at lower values of x. This investigation serves to show that if we use the asymptotic CDF representation in (18) to derive a simplified ABEP expression, then a good match with simulation results can be expected.

Based on the above motivation, we may substitute (18) in (7) for $F_{\bar{J}}(x,\bar{\sigma},\bar{c})$, and arrive at:

$$P_e \approx \frac{e^{\frac{\sigma^2}{2c^2}}}{2^N b^N (N-1)!}\int_0^{\infty} e^{\frac{-x^2}{2b}-\frac{x}{\bar{c}}}x^{2N-1}\mathrm{d}x. \tag{19}$$

Using [15, Equ. (3.462.1)], (19) is reduced to:

$$P_e \approx \frac{e^{\frac{\sigma^2}{2c^2}}}{2^N(N-1)!}\Gamma(2N)\exp\left(\frac{b}{4\bar{c}^2}\right)D_{-2N}\left(\frac{\sqrt{b}}{\bar{c}}\right). \tag{20}$$

It is immediately evident that the ABEP in (20) is significantly simpler than (17) to evaluate, since the confluent hypergeometric function is evaluated only once, while it is evaluated $N(2k+1)[3+2(n-1)]$ times in (17). Based on the previous motivation drawn from Fig. 3, the ABEP in (20) is also expected to agree well with simulation results at moderate-to-high SNRs. Comparison will be drawn in Section IV to demonstrate the accuracy of the expression.

2) ASYMPTOTIC ABEP

Based on the expression derived in (20), and applying the asymptotic representation of the parabolic cylinder function $D_{-v}(\cdot)$ using [15, Equ. (9.246.1)], we have:

$$P_e^{\gamma\to\infty}$$
$$\approx \frac{e^{\frac{\sigma^2}{2c^2}}}{2^N(N-1)!}\Gamma(2N)\left(\frac{\sqrt{b}}{\bar{c}}\right)^{-2N}\Bigg[1$$
$$-\frac{N(2N+1)\bar{c}^2}{b}+\frac{N(2N+1)(2N+2)(2N+3)\bar{c}^4}{4b^2}-\cdots\Bigg]. \tag{21}$$

Since $\bar{c}=\frac{c}{\sqrt{\gamma P_L N}}$ and $\gamma \to \infty$, the second and higher order terms will become very small and may thus be neglected, yielding the asymptotic ABEP:

$$P_e^{\gamma\to\infty} \approx \frac{e^{\frac{\sigma^2}{2c^2}}}{2^N(N-1)!}\Gamma(2N)\left(\frac{\sqrt{b}}{\bar{c}}\right)^{-2N}. \tag{22}$$

The result in (22) will be evaluated in Section IV.

3) DIVERSITY ORDER

Given the average SNR δ, the diversity order may be defined as: $G_d = \lim_{\delta\to\infty} -\frac{\log P_e}{\log \delta}$ and consequently $P_e^{\delta\to\infty} \approx \delta^{-G_d}$.

In order to determine the diversity order, we consider $\gamma \to \infty$. Substituting $\bar{c} = \frac{c}{\sqrt{\gamma P_L N}}$ and using $\delta = \frac{\gamma}{\sigma^2}$, (22) may be written as:

$$P_e^{\delta\to\infty} \approx \frac{e^{\frac{\sigma^2}{2c^2}}}{2^N(N-1)!}\Gamma(2N)\left(\frac{\sqrt{bP_L N}\sigma}{c}\right)^{-2N}\delta^{-N}. \quad (23)$$

It is immediately evident that the diversity order is given by $G_d = N$, and consequently does not affect the asymptotic diversity order of the AP-RIS in the presence of Gaussian-only additive noise [12].

C. TWO-WAY RELAYING

Two-way relaying employing physical-layer network coding is well-known [16] and enables two source nodes to exchange information via a relay node over two transmission phases. Two-way relaying has been considered for wireless communications to achieve spectrum efficiency gain and improved error performance as well as to extend network coverage, reduce shadowing effects, and increase power efficiency [16], [17].

Consider AP-RIS transceivers at Nodes A and B and a single-antenna transceiver at Node R as depicted in Fig. 4. Each of the nodes operate in half-duplex and the RISs are each equipped with N elements.

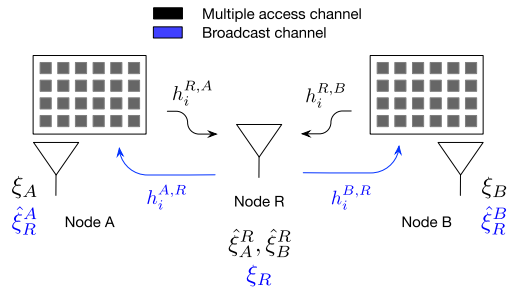

FIGURE 4. System model of the AP-RIS-assisted two-way relaying network.

In the multiple access channel (MAC) phase, Nodes A and B transmit their message symbols to Node R. Node R detects the two symbols and in the broadcast channel (BC) phase, transmits a network-coded version of the message symbols using decode-and-forward to Nodes A and B. Each of the nodes detect the received symbol and then perform network coding with their respective transmitted symbols. Hence the exchange of messages between Nodes A and B is achieved. Perfect transmit synchronization is assumed and that transmission from Node A cannot directly arrive at Node B or vice-versa due to large-scale fading. These assumptions are consistent with related literature [16], [17].

Accordingly, assuming a Rayleigh frequency-flat slow fading channel with path loss in the presence of Gaussian-plus-Laplacian additive noise, the received signal at Node R in the MAC phase is:

$$y_R = \sqrt{\gamma_A P_{L_A}}\sum_{i=1}^{N} h_i^{R,A} e^{j\phi_i^{R,A}}\xi_A + \sqrt{\gamma_B P_{L_B}}\sum_{i=1}^{N} h_i^{R,B} \times e^{j\phi_i^{R,B}}\xi_B + J_R, \quad (24.1)$$

$$= \sqrt{\gamma_A P_{L_A}}\sum_{i=1}^{N} \alpha_i^{R,A}\xi_A + \sqrt{\gamma_B P_{L_B}}\sum_{i=1}^{N} \alpha_i^{R,B}\xi_B + J_R, \quad (24.2)$$

where $h_i^{R,A(B)} = \alpha_i^{R,A(B)} e^{j\theta_i^{R,A(B)}}$ is the channel gain between the relay antenna and the i-th RIS element at Node A(B), with $\alpha_i^{R,A(B)}$ the respective channel magnitude and $\theta_i^{R,A(B)}$ the respective channel phase. In order to maximize the received SNR, the phase at each RIS is intelligently adjusted as $\phi_i^{R,A(B)} = -\theta_i^{R,A(B)}$, hence yielding (24.2). The symbol $\xi_{A(B)}$ is the assumed BPSK symbol emitted from Node A(B) with $E\{\xi_{A(B)}^2\} = 1$ and $\xi_{A(B)} \in \chi$. $\gamma_{A(B)}$ is the average transmit power at Node A(B). $P_{L_{A(B)}}$ is the total path loss with respect to Node A(B). $J_R = I_R + \eta_R$ with the mutually independent Laplacian and Gaussian additive noises represented by I_R and η_R, respectively.

Given complete knowledge of the channel, the symbols ξ_A, ξ_B detected at the relay node is determined as:

$$\left[\hat{\xi}_A^R, \hat{\xi}_B^R\right] = \underset{\xi_{A(B)}\in\chi}{\operatorname{argmin}}\left\{(y_R - \sqrt{\gamma_A P_{L_A}}\sum_{i=1}^{N}\alpha_i^{R,A}\xi_A - \sqrt{\gamma_B P_{L_B}}\sum_{i=1}^{N}\alpha_i^{R,B}\xi_B)^2\right\}, \quad (25)$$

Given the bit representation $b_{\hat{\xi}_{A(B)}^R}$ for the detected symbol $\hat{\xi}_{A(B)}^R$, network coding is applied at the relay as: $b_{\xi_R} = b_{\hat{\xi}_A^R} \oplus b_{\hat{\xi}_B^R}$. The corresponding assumed BPSK symbol $\xi_R \in \chi$ with $E\{\xi_R^2\} = 1$ is then transmitted by Node R in the BC phase. The received signal and subsequent detection rule (assuming complete knowledge of the channel) at Node A(B) are given as (26.1), (26.2) and (26.3), respectively.

$$y_{A(B)} = \sqrt{\gamma_R P_{L_{A(B)}}}\sum_{i=1}^{N} h_i^{A(B),R} e^{j\phi_i^{A(B),R}}\xi_R + J_{A(B)} \quad (26.1)$$

$$= \sqrt{\gamma_R P_{L_{A(B)}}}\sum_{i=1}^{N} \alpha_i^{A(B),R}\xi_R + J_{A(B)}, \quad (26.2)$$

$$\hat{\xi}_R^{A(B)} = \underset{\xi_R\in\chi}{\operatorname{argmin}}\left\{(y_{A(B)} - \sqrt{\gamma_R P_{L_{A(B)}}}\sum_{i=1}^{N}\alpha_i^{A(B),R}\xi_R)^2\right\}, \quad (26.3)$$

where $h_i^{A(B),R} = \alpha_i^{A(B),R} e^{j\theta_i^{A(B),R}}$ is the Rayleigh frequency-flat slow fading channel gain between the i-th RIS element at Node A(B) and Node R, with $\alpha_i^{A(B),R}$ the respective channel magnitude and $\theta_i^{A(B),R}$ the respective channel phase. In order to maximize the received SNR, the phase at each RIS is

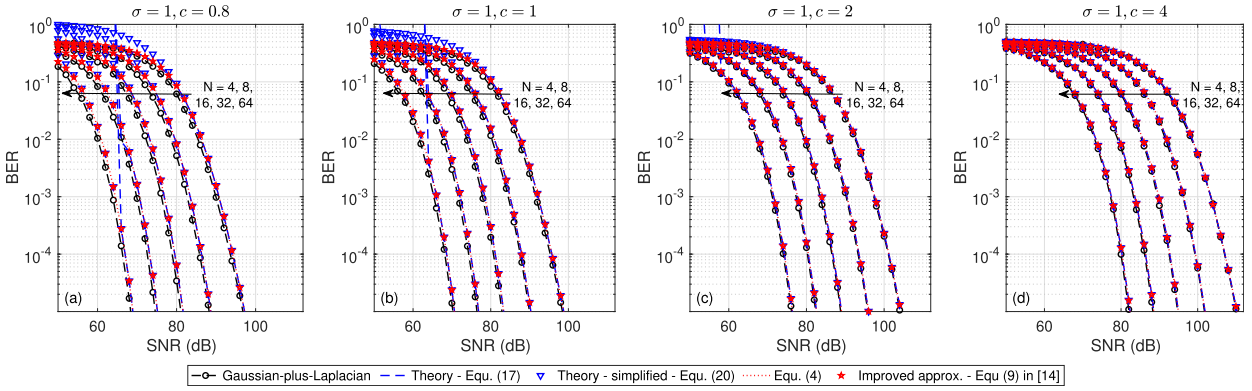

FIGURE 5. Validation of error performance for AP-RISs ($N = 4, 8, 16, 32$ and 64) for $\sigma = 1$, $c = 0.8, 1, 2$ and 4 with $r_1 = 1$ m and $r_2 = 9$ m.

intelligently adjusted as $\phi_i^{A(B),R} = -\theta_i^{A(B),R}$, hence yielding (26.2). γ_R is the average transmit power at the relay. $P_{L_{A(B)}}$ is the total path loss with respect to Node A(B). $J_{A(B)} = I_{A(B)} + \eta_{A(B)}$, where the mutually independent Laplacian and Gaussian additive noises are represented by $I_{A(B)}$ and $\eta_{A(B)}$, respectively, at Node A(B).

Finally, the bit representation $b_{\hat{\xi}_{B(A)}} = b_{\hat{\xi}_R^{A(B)}} \oplus b_{\xi_{A(B)}}$ is determined at Node A(B), hence achieving the exchange of message symbols between Nodes A and B.

1) ERROR PERFORMANCE

Consider the transmission from Node A(B) to Node B(A), then based on the analysis of the error performance of two-way relaying presented in [17], the ABEP may be expressed as:

$$P_e^{A(B)\to B(A)} \approx P_{e_A}^{A,B\to R} + P_{e_B}^{A,B\to R} - [2((P_{e_A}^{A,B\to R} + P_{e_B}^{A,B\to R}) - 1]P_e^{R\to B(A)}, \quad (27)$$

where $P_{e_{A(B)}}^{A,B\to R}$ is the error probability at the relay assuming $\xi_{A(B)}$ is received in error, while $\xi_{B(A)}$ is received correctly and $P_e^{R\to B(A)}$ is the error probability at Node B(A).

Assuming each node employs the transmission of a BPSK symbol, then the probabilities on the RHS of (27) may be given as P_e in (17); hence, (27) may be simplified as:

$$P_e^{A(B)\to B(A)} \approx 3P_e - 4P_e^2. \quad (28)$$

We may also employ the simplified ABEP given by (20) for P_e in (28). Both results will be plotted and compared in Section IV.

IV. NUMERICAL RESULTS

In this section, we first present the numerical results for the AP-RIS assuming a Rayleigh frequency-flat slow fading channel with path loss in the presence of Gaussian-plus-Laplacian additive noise. Second, we present the numerical results for AP-RIS-assisted two-way relaying under the same channel conditions. For error performance comparisons, the figure-of-merit considered is the bit error rate (BER) versus average SNR. We consider the average SNR $\delta = \frac{\gamma}{\sigma^2}$ with $\gamma = \gamma_A = \gamma_B = \gamma_R$. Comparisons are drawn at a BER of 10^{-5} unless otherwise stated. We consider $N = 4, 8, 16, 32$ and 64. BPSK modulation is assumed. Values of $c = 0.8, 1, 2$ and 4 are considered. In all cases, we assume $\sigma = 1$. For large-scale fading, the total path loss P_L is defined as [5], [6]:

$$P_L = \frac{\lambda^4}{256(\pi r_1 r_2)^2}, \quad (29)$$

where $\lambda = c/f_c$, with c the speed of light, f_c is the carrier frequency, r_1 is the distance between the transmit antenna and AP-RIS and r_2 is the distance between the AP-RIS and receive antenna. For two-way relaying, we consider $P_L = P_{L_A} = P_{L_B}$, r_1 the distance between the transmit antenna and AP-RIS at Node A(B), r_2 the distance between the AP-RIS at Node A(B) and antenna at Node R. In the following results, we choose $f_c = 1.8$ GHz, $r_1 = 1$ m, $r_2 = 9$ m or $r_1 = 1$ m, $r_2 = 12$ m.

A. AP-RISs IN THE PRESENCE OF GAUSSIAN-PLUS-LAPLACIAN ADDITIVE NOISE

In Fig. 5 (refer to the top of next page), the simulation results and evaluated theoretical ABEP curves given by (17) and (20) are presented. We have also included the MATLAB symbolic math toolbox integrations of (4) with $f_x(x)$ given by (5) and its improved approximation (cf. Equ. (9) in [14]). We have considered the CDF given by (6) for these integrations. In all settings of c and N, it is evident that the theoretical and simulation results agree well at moderate-to-high SNRs and are valid even for small RISs. More specifically, for $c = 0.8$ and 1 (Figs. 5(a) and (b)), the results agree well at moderate-to-high SNRs, while for heavier noise tails with $c = 2$ and 4 (Figs. 5(c) and (d)), simulation and theoretical results increase in tightness and generally agree well across the range of SNRs. However, only in some of these instances do they match at low SNRs. This will be discussed in brief shortly. In all settings of N, the simplified ABEP given in (20) matches the ABEP of (17) and the simulation results very closely for moderate-to-high SNRs for $c = 0.8, 1$ and for low-to-high SNRs for $c = 2$, $c = 4$. It is also demonstrated that the curves plotted for (4) match the derived ABEP exactly at

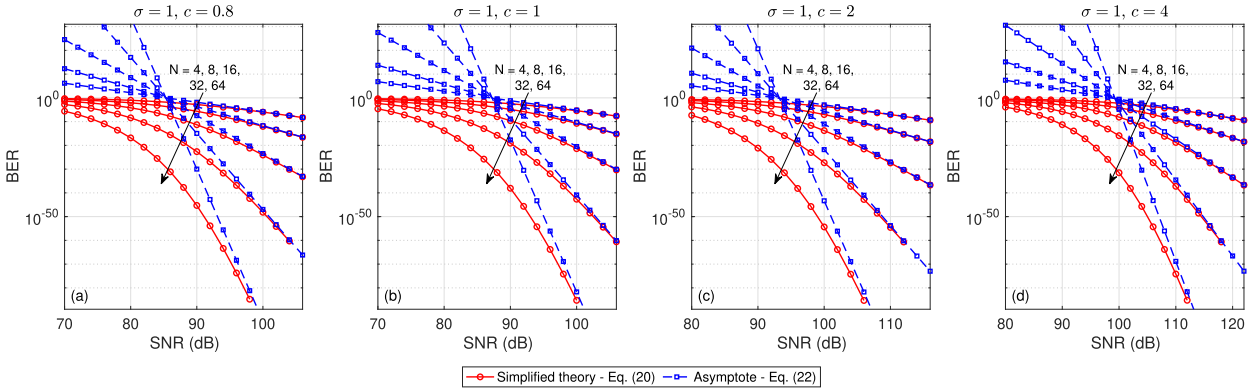

FIGURE 6. Asymptotic ABEP for $\sigma = 1$, $c = 0.8$, 1, 2, 4, $N = 4$, 8, 16, 32 and 64 with $r_1 = 1$ m and $r_2 = 9$ m.

moderate-to-high SNRs in the cases of $c = 0.8$ and 1 and at low-to-high SNRs for the cases of $c = 2$ and $c = 4$. Furthermore, the improved approximation of $f_x(x)$ presented in [14], demonstrates no further improvement in accuracy of the ABEP. As mentioned earlier, in some instances it is evident that there is difference between the ABEP of (17), simplified ABEP of (20) and simulation results at low SNRs. At the same time, the curves for (4) and the improved approximation for $f_x(x)$ matches the simulation results much more closely at these low SNRs. Based on this, we can state that the error is not due to the Gaussian-plus-Laplacian noise CDF employed at low values of c. This is further evidenced in the comparisons drawn in Figure 2. Instead, since the error at low SNRs is much more pronounced for (17) and significantly less for (20), we can induce that such error is due to the inaccuracy of the confluent hypergeometric function computation at these SNRs.

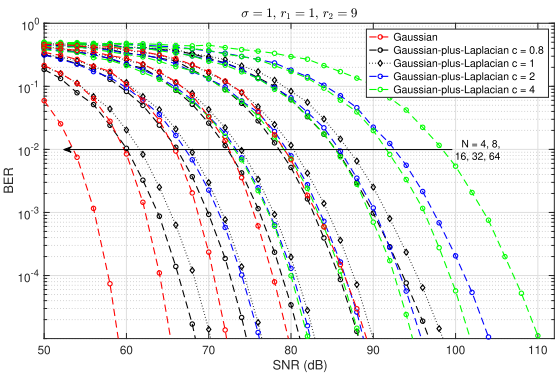

FIGURE 7. Comparison of error performance for AP-RISs ($N = 4$, 8, 16, 32 and 64) with Gaussian-only ($\sigma = 1$) and Gaussian-plus-Laplacian ($\sigma = 1$, $c = 0.8$, 1, 2 and 4) additive noise.

Fig. 6 (refer to top of next page) presents the BER vs. SNR result in order to draw comparison with the asymptotic ABEP given by (22). Since it is not practical to obtain the simulation results at the high SNRs of interest, we have instead generated the curves using the simplified ABEP given by (20). Results have been shown for $N = 4$, 8, 16, 32 and 64 with $\sigma = 1$, $c = 0.8$, 1, 2, 4 and we consider $r_1 = 1$ m and $r_2 = 9$ m. In each of the cases, it is evident that the curves converge and a close match is seen at high SNRs. Using (22), the asymptotic diversity order was shown earlier to be $G_d = N$. Since the curves converge and the slopes are identical at high SNRs, the diversity order is evident.

In Fig. 7, comparison is drawn between the error performances with and without the impulsive noise component. Serious degradation is shown when the noise includes an impulsive component. This is even more so when the noise tails become heavier ($c = 1$, 2 and 4). For example, considering $N = 64$, SNR penalties of approximately 9.5 dB are evident for $c = 0.8$, while approximately 11 dB, 17 dB and 23 dB penalties are evident for $c = 1$, $c = 2$ and $c = 4$, respectively. Similar penalties are evident for other values of N and are tabulated in Table 1.

TABLE 1. Summary of SNR penalties due to impulsive noise component for $N = 4$, 8, 16, 32 and 64 with $\sigma = 1$ and $c = 0.8$, 1, 2 and 4.

N	SNR penalty (dB)			
	$\sigma = 1, c = 0.8$	$\sigma = 1, c = 1$	$\sigma = 1, c = 2$	$\sigma = 1, c = 4$
4	7.5	9.2	14.5	20.5
8	8.8	10.6	16.4	22.2
16	8.9	11.0	16.7	22.0
32	9.0	11.0	16.6	22.0
64	9.5	11.3	17.1	23.3

B. AP-RIS-ASSISTED TWO-WAY RELAYING

Figs. 8 and 9 present the simulation results and evaluated theoretical ABEPs for the AP-RIS-assisted two-way relaying network. Comparison is drawn between the error performances with and without the impulsive noise component. We consider $\sigma = 1$ and $c = 1$. Two configurations $r_1 = 1$ m, $r_2 = 9$ m and $r_1 = 1$ m, $r_2 = 12$ m are considered.

Severe penalties in SNR are evident in the presence of noise with an impulsive component. For example, in Figs. 8 and 9, for $N = 64$ there is a penalty of approximately 11 dB, while similar penalties are evident for other values of N. In each instant, it is evident that the theoretical ABEP, which

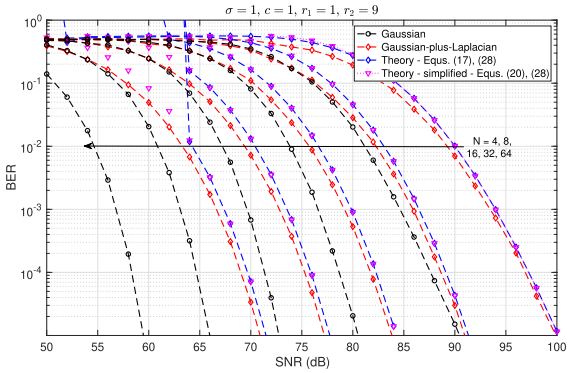

FIGURE 8. Comparison of error performance for AP-RIS-assisted two-way relaying ($N = 4, 8, 16, 32$ and 64) with Gaussian-only ($\sigma = 1$) and Gaussian-plus-Laplacian ($\sigma = 1$, $c = 1$) additive noise for $r_1 = 1$ m and $r_2 = 9$ m.

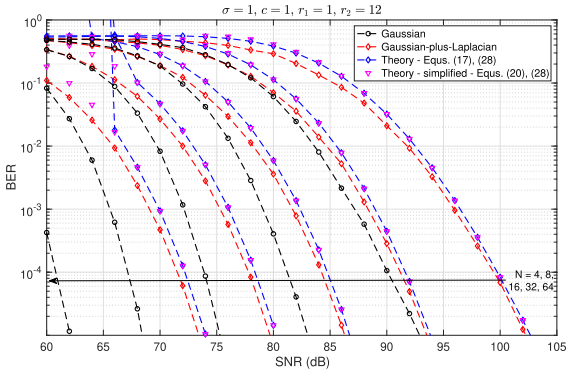

FIGURE 9. Comparison of error performance for AP-RIS-assisted two-way relaying ($N = 4, 8, 16, 32$ and 64) with Gaussian-only ($\sigma = 1$) and Gaussian-plus-Laplacian ($\sigma = 1$, $c = 1$) additive noise for $r_1 = 1$ m and $r_2 = 12$ m.

is a bound [17] given by (17) in (28), agrees well with the simulation results. The simplified ABEP using (20) in (28) also agrees very well and is identical to (28) using (17) at higher SNRs.

V. CONCLUSION AND FUTURE WORK

In this paper, the error performance of an AP-RIS in the presence of Gaussian-plus-Laplacian additive noise was investigated. The formulated theoretical ABEP was validated by simulation results and allows arbitrary RIS sizes. A simplified ABEP that requires only a single evaluation of the confluent hypergeometric function was derived and matched simulation results well. Both formulations were used in the validation of the error performance of an AP-RIS-assisted two-way relaying network. Results presented in this paper demonstrate the vulnerability of RISs to additive noise with an impulsive component. Future work involves the investigation of techniques to mitigate the deleterious impact this type of noise has on the error performance of RIS-based communications. The effects of co-channel interference may also be investigated together with extending the result to generalized channels.

APPENDIX A
DERIVATION OF INTEGRAL $\mathcal{I}_1$

Given $\mathcal{I}_1 = \int_0^\infty x^{2N-1} e^{-\frac{x^2}{2b}} F_{\bar{J}}(x, \bar{\sigma}, \bar{c}) \mathrm{d}x$, let $u = F_{\bar{J}}(x, \bar{\sigma}, \bar{c})$ and $\mathrm{d}v = x^{2N-1} e^{-\frac{x^2}{2b}} \mathrm{d}x$. Using [15, Equ. (2.33.11)]:

$$v = -\frac{(N-1)!}{2} e^{-\frac{x^2}{2b}} \sum_{k=0}^{N-1} \frac{x^{2k}}{k! \left(\frac{1}{2b}\right)^{N-k}}. \tag{30}$$

We then have:

$$\begin{aligned}\mathcal{I}_1 &= -F_{\bar{J}}(x, \bar{\sigma}, \bar{c}) \frac{(N-1)!}{2} e^{-\frac{x^2}{2b}} \sum_{k=0}^{N-1} \frac{x^{2k}}{k! \left(\frac{1}{2b}\right)^{N-k}} \Bigg|_0^\infty \\ &\quad + \frac{(N-1)!}{2} \sum_{k=0}^{N-1} \frac{1}{k! \left(\frac{1}{2b}\right)^{N-k}} \int_0^\infty x^{2k} e^{-\frac{x^2}{2b}} f_{\bar{J}}(x, \bar{\sigma}, \bar{c}) \mathrm{d}x.\end{aligned} \tag{31}$$

Since $F_{\bar{J}}(0, \bar{\sigma}, \bar{c}) = \frac{1}{2}$, (31) is reduced to:

$$\begin{aligned}\mathcal{I}_1 = \frac{(N-1)!}{2^{2-N} b^{-N}} + \frac{(N-1)!}{2} \sum_{k=0}^{N-1} \frac{1}{k! \left(\frac{1}{2b}\right)^{N-k}} \\ \times \int_0^\infty x^{2k} e^{-\frac{x^2}{2b}} f_{\bar{J}}(x, \bar{\sigma}, \bar{c}) \mathrm{d}x.\end{aligned} \tag{32}$$

APPENDIX B
DERIVATION OF INTEGRAL $\mathcal{I}_2$

It may be validated that $\mathcal{I}_2 = \int_0^\infty x^{2k} e^{-\frac{x^2}{2b}} f_{\bar{J}}(x, \bar{\sigma}, \bar{c}) \mathrm{d}x$, may be written as:

$$\mathcal{I}_2 = \frac{1}{2\bar{c}} e^{\frac{\sigma^2}{2c^2}} \int_{-\infty}^\infty x^{2k} e^{-\frac{x^2}{2b}} e^{\frac{x}{c}} Q\left(\frac{x}{\bar{\sigma}} + \frac{\sigma}{c}\right) \mathrm{d}x. \tag{33}$$

Let $y = \frac{x}{\bar{\sigma}} + \frac{\sigma}{c}$, $\varphi_1 = \frac{\bar{\sigma}^2}{b}$ and $\varphi_2 = \frac{\sigma}{c}$, then simplifying and rearranging, we have:

$$\begin{aligned}\mathcal{I}_2 = \frac{1}{2\bar{c}} e^{-0.5\varphi_2^2(\varphi_1+1)} \bar{\sigma}^{2k+1} \\ \times \int_{-\infty}^\infty e^{-0.5\varphi_1 y^2} e^{\varphi_2(\varphi_1+1)y} (y - \varphi_2)^{2k} Q(y) \mathrm{d}y.\end{aligned} \tag{34}$$

Using the binomial expansion for $(y - \varphi_2)^{2k}$, given as:

$$(y - \varphi_2)^{2k} = \sum_{m=0}^{2k} (-1)^{2k-m} \binom{2k}{m} y^m \varphi_2^{2k-m}, \tag{35}$$

we have:

$$\begin{aligned}\mathcal{I}_2 = \frac{1}{2\bar{c}} e^{-0.5\varphi_2^2(\varphi_1+1)} \bar{\sigma}^{2k+1} \sum_{m=0}^{2k} (-1)^{2k-m} \binom{2k}{m} \varphi_2^{2k-m} \\ \times \int_{-\infty}^\infty e^{-0.5\varphi_1 y^2} e^{\varphi_2(\varphi_1+1)y} y^m Q(y) \mathrm{d}y\end{aligned} \tag{36}$$

REFERENCES

[1] Y.-C. Liang, R. Long, Q. Zhang, J. Chen, H. V. Cheng, and H. Guo, "Large intelligent surface/antennas (LISA): Making reflective radios smart," *J. Commun. Inf. Netw.*, vol. 4, no. 2, pp. 40–50, Jun. 2019.
[2] J. Zhao, "A survey of intelligent reflecting surfaces (IRSs): Towards 6G wireless communication networks," 2019, *arXiv:1907.04789*.
[3] X. Yuan, Y.-J. A. Zhang, Y. Shi, W. Yan, and H. Liu, "Reconfigurable-intelligent-surface empowered wireless communications: Challenges and opportunities," 2020, *arXiv:2001.00364*.
[4] A. Sikri, A. Mathur, P. Saxena, M. R. Bhatnagar, and G. Kaddoum, "Reconfigurable intelligent surface for mixed FSO-RF systems with co-channel interference," *IEEE Commun. Lett.*, vol. 25, no. 5, pp. 1605–1609, May 2021.
[5] A. Khaleel and E. Basar, "Reconfigurable intelligent surface-empowered MIMO systems," *IEEE Syst. J.*, vol. 15, no. 3, pp. 4358–4366, Sep. 2021.
[6] S. W. Ellingson, "Path loss in reconfigurable intelligent surface-enabled channels," 2019, *arXiv:1912.06759*.
[7] X. Tang, D. Wang, R. Zhang, Z. Chu, and Z. Han, "Jamming mitigation via aerial reconfigurable intelligent surface: Passive beamforming and deployment optimization," *IEEE Trans. Veh. Technol.*, vol. 70, no. 6, pp. 6232–6237, Jun. 2021.
[8] E. Basar, "Transmission through large intelligent surfaces: A new frontier in wireless communications," in *Proc. Eur. Conf. Netw. Commun. (EuCNC)*, Jun. 2019, pp. 112–117.
[9] B. Selim, M. S. Alam, G. Kaddoum, and B. L. Agba, "Effect of impulsive noise on uplink NOMA systems," *IEEE Trans. Veh. Technol.*, vol. 69, no. 3, pp. 3454–3458, Mar. 2020.
[10] L. Clavier, G. W. Peters, F. Septier, and I. Nevat, "Impulsive noise modeling and robust receiver design," *EURASIP J. Wireless Commun. Netw.*, vol. 2021, no. 1, pp. 1–30, Dec. 2021.
[11] S. Niranjayan and N. C. Beaulieu, "Analysis of wireless communication systems in the presence of non-Gaussian impulsive noise and Gaussian noise," in *Proc. IEEE Wireless Commun. Netw. Conf.*, Apr. 2010, pp. 1–6.
[12] N. Pillay and H. Xu, "Reconfigurable intelligent surface-aided single-input single-output K-complex symbol golden codeword-based modulation," *IEEE Access*, vol. 9, pp. 71849–71855, 2021, doi: 10.1109/ACCESS.2021.3078884.
[13] N. Beaulieu and S. Niranjayan, "UWB receiver designs based on a Gaussian-Laplacian noise-plus-MAI model," *IEEE Trans. Commun.*, vol. 58, no. 3, pp. 997–1006, Mar. 2010.
[14] J. Hu and N. C. Beaulieu, "Accurate simple closed-form approximations to Rayleigh sum distributions and densities," *IEEE Commun. Lett.*, vol. 9, no. 2, pp. 109–111, Feb. 2005.
[15] I. S. Gradshteyn and I. M. Ryzhik, *Table of Integrals, Series, and Products*, 7th ed. Amsterdam, The Netherlands: Elsevier, 2007.
[16] H. Ju, E. Oh, and D. Hong, "Catching resource-devouring worms in next-generation wireless relay systems: Two-way relay and full-duplex relay," *IEEE Commun. Mag.*, vol. 47, no. 9, pp. 58–65, Sep. 2009.
[17] S. Althunibat and R. Mesleh, "Performance analysis of quadrature spatial modulation in two-way relaying cooperative networks," *IET Commun.*, vol. 12, no. 4, pp. 466–472, 2018.

NARUSHAN PILLAY (Member, IEEE) received the M.Sc.Eng. *(cum laude)* and Ph.D. degrees in wireless communications from the University of KwaZulu-Natal, Durban, South Africa, in 2008 and 2012, respectively. Since 2009, he has been with the University of KwaZulu-Natal. Previously, he was with the Council of Scientific and Industrial Research (CSIR), Defence, Peace, Safety and Security (DPSS), South Africa. He has published several articles in well-known journals in his area of research. He currently supervises several Ph.D. and M.Sc.Eng. students. He is an NRF-Rated Researcher in South Africa. His research interests include physical wireless communications, including spectrum sensing for cognitive radio and MIMO systems.

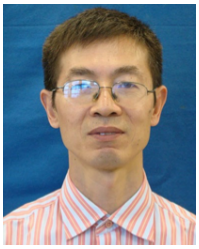

HONGJUN XU (Member, IEEE) received the B.Sc. degree from the Guilin University of Electronic Technology, China, in 1984, the M.Sc. degree from the Institute of Telecontrol and Telemeasure, Shijianzhuang, China, 1989, and the Ph.D. degree from the Beijing University of Aeronautics and Astronautics, Beijing, China, in 1995. From 1997 to 2000, he was a Postdoctoral Researcher at the University of Natal and Inha University. He is currently a Full Professor with the School of Engineering, University of KwaZulu-Natal, Howard College Campus. He is also a National Research Foundation (NRF) Rated Researcher in South Africa. He has published more than 50 journal articles. His research interests include digital and wireless communications and digital systems.